Experiments in Fluids 26 (1999) 215–221 © Springer-Verlag 1999

Kinematic characteristics of magnetic fluid sloshing in a rectangular container subject to non-uniform magnetic fields

T. Sawada, H. Kikura, T. Tanahashi

Abstract The dynamic behavior of a magnetic fluid in a laterally vibrated rectangular container subject to a non-uniform vertical magnetic field has been investigated. Flow behavior was observed using the ultrasound velocity profile measuring technique. The effect of the magnetic field on the resonant frequency of the fluid-container system is discussed. Experimental results are compared with the results obtained from nonlinear theory using the perturbation method.

1 Introduction

A magnetic fluid is a stable suspension of solid magnetic particles whose diameter is 5 ~ 15 nm. The particles are coated with a layer of surfactant which inhibits their coalescence, that is, the magnetic fluid is a stable colloidal dispersion of rather small surfactant-coated magnetic particles in a liquid carrier. When a magnetic field is applied to a magnetic fluid, the magnetic particles in the fluid tend to remain rigidly aligned with the orientation of the magnetic field, and several interesting characteristics have been observed (e.g. Rosensweig 1985).

Zelazo and Melcher (1969) investigated the dynamic behavior of a magnetic fluid in an oscillated container. They examined the influence of a tangential magnetic field on the resonance of surface waves, using a rectangular container partly filled with a magnetic fluid and driven by a low-frequency transducer. Also, a simulation of liquid sloshing in low-gravity were demonstrated by Dodge and Garza (1970) using a magnetic fluid. More recently, interfacial instability of a magnetic fluid in an applied magnetic field has attracted attention. Sudo et al. (1987) carried out an experimental study on the interfacial instability of magnetic fluids in a rectangular container in the presence of a magnetic field tangential to the interface and estimated the concrete configurations of the interface in various conditions. Okubo et al. (1990) investigated the stability of the surface of a magnetic fluid layer under the influence of a vertical alternating magnetic field. Kikura et al. (1991) examined lateral sloshing of a magnetic fluid in rectangular, cylindrical and spherical containers. From these studies several characteristic properties of magnetic fluid sloshing have been clarified, for example, the effects of magnetic field on the resonant frequency and change of pressure.

Further studies have investigated the sloshing of two fluid layers (e.g. Handa and Tajima 1979). Li (1970) analyzed the stability of two liquid layers with a free surface set in motion by an oscillatory lower boundary, using two superposed fluids with different viscosities and densities. He pointed out that there are two modes of wave motion. Hashimoto and Sudo (1985) presented a linearized three-dimensional theory of the waves occurring on the free surface and liquid–liquid interface taking account of surface tension. They carried out some experiments and investigated the dynamic behavior of stratified fluids with a free surface in a rectangular container subject to vertical vibration. Sawada et al. (1993) and Matsuura et al. (1995) investigated a two-layer liquid sloshing of a magnetic fluid and silicon oil in a rectangular container, and clarified the effects of a magnetic field on the resonant frequency.

The sloshing problem is not easy from a mathematical point of view. Nonlinearities occur, especially in the vicinity of the resonant frequency. In order to understand and explain this complex problem, a nonlinear approach and detailed measurement of internal velocity profiles are necessary. However, optical methods like laser Doppler anemometry or the flow visualization techniques like particle image velocimetry can not be applied because magnetic fluids are opaque. For this reason, most of the experimental investigations have been concerned with the measurement of pressure distribution and observation of the free surface. Thus the internal velocity and the velocity profile measurement has long been called for.

In the present paper, we investigate the magnetic fluid sloshing in a rectangular container subject to a non-uniform vertical magnetic field by the nonlinear perturbation method. We calculate nonlinear sloshing responses up to the third order perturbation. We attempt to measure the velocity profile of the magnetic fluid sloshing, using the ultrasound Doppler

Received: *27 May 1997*/*Accepted*: *26 March 1998*

T. Sawada, T. Tanahashi
Department of Mechanical Engineering, Keio University
3-14-1 Hiyoshi, Kohoku-ku, Yokohama 223-8522, Japan

H. Kikura
Paul Scherrer Institute, CH-5232 Villigen PSI, Switzerland

Correspondence to: T. Sawada

We would like to thank Prof. Y. Kurosaki (Tokyo Institute of Technology, Japan) for his assistance with UVP measurements. We wish to express our gratitude to Dr. Y. Takeda (Paul Scherrer Institute, Switzerland) for his collaboration in this work. We also acknowledge the assistance of F. Matsuura and G. Yamanaka during the experiment.

A version of this paper was presented at the First International Symposium on Ultrasound Doppler Methods, Villigen, Switzerland, 1996.

velocimetry in order to examine theoretical results. Ultrasound Doppler velocimetry is a method of measuring a velocity profile along a beam line; that is, with respect to the velocity component along the ultrasound beam. This method can be applied to opaque fluids such as a liquid metal. Takeda (1986) has developed the Ultrasound Velocity Profile (UVP) monitor over past 10 years and has studied its application to the flow of mercury (Takeda 1987). Though UVP method is very useful technique, it has been hardly used for measuring a velocity profile of magnetic fluids. We examine the applicability of this method to magnetic fluid sloshing which has periodic velocity field, and the experimental and nonlinear theoretical results are compared.

2 Experiments

Figure 1 shows the schematic diagram of the experimental apparatus. The rectangular container measures 80 mm × 20 mm × 150 mm (see Fig. 2), and is made of transparent acrylic resin. An adjustable crank is mounted on the output shaft of the motor. The rotational frequency of the motor is continuously controlled by an inverter. The table is oscillated sinusoidally and has a range of oscillation from 1.17 to 4.33 Hz. When the amplitude of oscillation is changed, the surface disturbance is also changed. But there is little influence of the excitation amplitude on the resonant frequency. Since we pay attention to the resonant sloshing behavior, the amplitude of oscillation is $X_0 = 1.5$ mm for all experiments. A magnetic field is generated by a cylindrical permanent magnet whose diameter is 110 mm. The distribution of the magnetic field induction B along the normal central line of the permanent magnet is shown in Fig. 3. Here h is the fluid depth, B_0 is the surface magnetic field induction at the center of the permanent magnet ($z = -h$), and h_m is the distance from the permanent magnet. The equation for B is obtained by measured results and is then used for theoretical analysis.

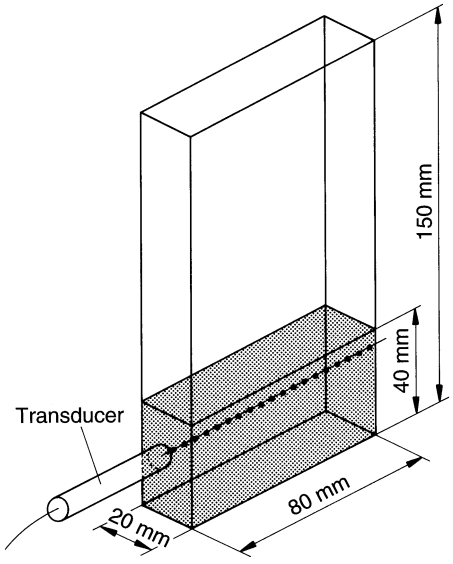

Fig. 2. Container

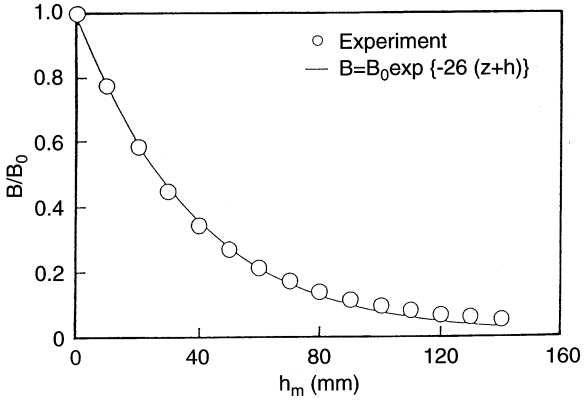

Fig. 3. Distribution of magnetic field induction along the normal central line of the permanent magnet

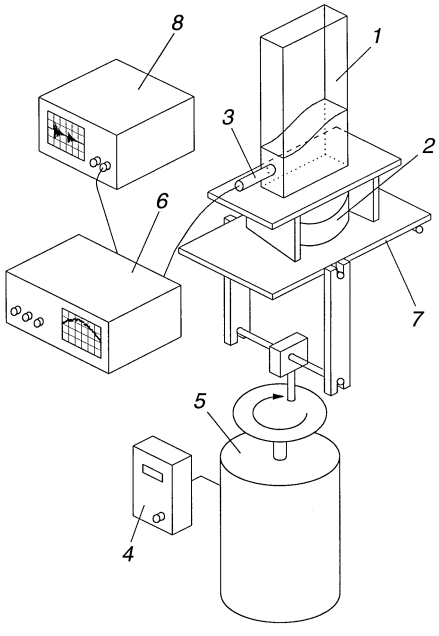

Fig. 1. Experimental apparatus. *1* Container, *2* magnet, *3* US transducer, *4* controller, *5* motor, *6* UVP monitor, *7* shaking table, *8* oscilloscope

The magnetic fluid is a water-based 24% weight concentration of fine magnetite particles, Fe_3O_4. Its kinematic viscosity, density and sound velocity are $\nu = 4.2 \times 10^{-6}$ m^2/s, $\rho = 1.24 \times 10^3$ kg/m^3 and $c = 1440$ m/s at 25 °C, respectively. The fluid depth is $h = 40$ mm. Since the magnetic particles in the magnetic fluid are too small to reflect ultrasonic waves, we also add porous SiO_2 powder with a mean diameter of 0.9 μm (MSF-10M, Liquidgas Co., Ltd.). An ultrasonic transducer is fixed on the side wall of the container in order to measure the horizontal velocity profile V_x. The ultrasonic transducer has an active diameter of 5 mm and the measuring volume is a thin-disc shape element, $\phi 5$ mm × 0.71 mm. The UVP monitor used is an Model X-1 PS manufactured by Met-Flow SA. The basic frequency is 4 MHz and the pulse repetition frequency is 3906 Hz.

Experiments were carried out at various motor frequencies and magnetic field intensities. The dynamic behavior of the free surface are recorded on video tape.

3 Nonlinear wave theory

Frequency responses of the free surface of a magnetic fluid have been investigated using linearized wave theory by Matsuura et al. (1995). However, the flow behavior of sloshing is essentially nonlinear. In particular, forced oscillation clearly shows nonlinear characteristics in its resonance curves. Thus, a nonlinear approach is necessary to investigate velocity fields and high frequency responses of the free surface. Here we deal with an analytical solution to sloshing subject to non-uniform magnetic field using a perturbation method (see Hayama et al. 1983). An analytical model uses the Cartesian coordinates x and z as shown in Fig. 4, x is horizontal while z is vertical upward measured from the mean position of the free surface. L is the length of the container and η is the free surface elevation. X_0 and ω are the amplitude and forced angular frequency of the oscillation of the shaking table, respectively.

With the assumptions of irrotational flow and an incompressible fluid, a velocity potential ϕ exists which should satisfy the continuity equation:

$$\frac{\partial^2\phi}{\partial x^2}+\frac{\partial^2\phi}{\partial z^2}=0 \tag{1}$$

The unsteady Bernoulli equation is given by

$$\frac{\partial\phi}{\partial t}+\frac{1}{2}\left\{\left(\frac{\partial\phi}{\partial x}\right)^2+\left(\frac{\partial\phi}{\partial z}\right)^2\right\}+\frac{p}{\rho}+gz-\mu_0\int_0^H M\,\mathrm{d}H = X_0\omega^2 x\sin\omega t \tag{2}$$

where p, g, μ_0, M and H are pressure, gravitational acceleration, magnetic permeability of vacuum, magnetization and magnetic field, respectively. When the magnetization and magnetic field are assumed to be parallel, the fifth term of the left hand side of Eq. (2) is written

$$\mu_0\int_0^H M\,\mathrm{d}H=\frac{1}{2}\mu_0\chi_m H^2 \tag{3}$$

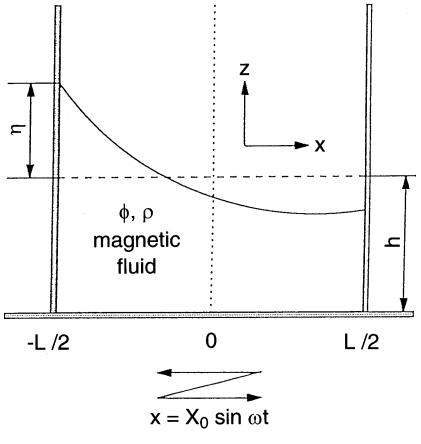

Fig. 4. Analytical model

where χ_m is susceptibility of a magnetic fluid. The magnetic field $H(z)$ is approximated by

$$H(z)=H_0\,\mathrm{e}^{-\alpha(z+h)} \tag{4}$$

where H_0 is the magnetic field intensity at the bottom of the container ($z=-h$) and α is a constant which is determined by measurement of the magnetic field as shown in Fig. 3. The boundary conditions on the bottom and side walls, and the kinematic and dynamic free surface conditions (e.g. Dean and Dalrymple 1984) are given by following equations:

$$\left(\frac{\partial\phi}{\partial x}\right)_{x=\pm L/2}=0 \tag{5}$$

$$\left(\frac{\partial\phi}{\partial z}\right)_{z=-h}=0 \tag{6}$$

$$\left(\frac{\partial\eta}{\partial t}+\frac{\partial\phi}{\partial x}\frac{\partial\eta}{\partial x}\right)_{z=\eta}=\left(\frac{\partial\phi}{\partial z}\right)_{z=\eta} \tag{7}$$

$$\left[\frac{\partial^2\phi}{\partial t^2}+2\left(\frac{\partial\phi}{\partial x}\frac{\partial^2\phi}{\partial x\partial t}+\frac{\partial\phi}{\partial z}\frac{\partial^2\phi}{\partial z\partial t}\right)+\left\{\left(\frac{\partial\phi}{\partial x}\right)^2\frac{\partial\phi}{\partial x^2}+\left(\frac{\partial\phi}{\partial z}\right)^2\frac{\partial^2\phi}{\partial z^2}\right\}+2\frac{\partial\phi}{\partial x}\frac{\partial\phi}{\partial z}\frac{\partial^2\phi}{\partial x\partial z}+g_m\frac{\partial\phi}{\partial z}-X_0\omega^3 x\cos\omega t-X_0\omega^2\frac{\partial\phi}{\partial x}\sin\omega t\right]_{z=\eta}=0 \tag{8}$$

where g_m is an effective gravity due to the magnetic force and is given by

$$g_m=g+\frac{\alpha\mu_0\chi_m H_0^2\,\mathrm{e}^{-2\alpha h}}{\rho} \tag{9}$$

Since Eqs. (7) and (8) for the free surface conditions are nonlinear, they are linearized by developing ϕ, η and p into power series of small parameter $\varepsilon=(X_0/L)^{1/3}$ up to the third order perturbation. These expressions are written in the following dimensionless form:

$$\phi^*=\frac{\phi}{L^2\omega_1}=\varepsilon\phi_1+\varepsilon^2\phi_2+\varepsilon^3\phi_3+O(\varepsilon^4) \tag{10}$$

$$\eta^*=\frac{\eta}{L}=\varepsilon\eta_1+\varepsilon^2\eta_2+\varepsilon^3\eta_3+O(\varepsilon^4) \tag{11}$$

$$p^*=\frac{p}{\rho gL}=-z^*+\varepsilon p_1+\varepsilon^2 p_2+\varepsilon^3 p_3+O(\varepsilon^4) \tag{12}$$

where ω_1 is the first resonant angular frequency obtained by linearized theory and where the function O represents other perturbation orders. The first resonant angular frequency ω_1 is given by the nth resonant angular frequency equation:

$$\omega_n=\sqrt{\frac{n\pi g_m}{L}\tanh\frac{n\pi h}{L}} \tag{13}$$

Space and time variables are also defined in dimensionless form:

$$x^*=\frac{x}{L},\quad z^*=\frac{z}{L},\quad t^*=\omega t \tag{14}$$

Since we are interested in the behavior at the vicinity of the resonant point, we write angular frequency ω as follows:

$$\frac{\omega}{\omega_1}=1+\varepsilon\alpha_1+\varepsilon^2\alpha_2+O(\varepsilon^2) \tag{15}$$

Using the preparations, Eqs. (7) and (8) are linearized and we obtain the following nonlinear solutions:

$$\phi_1=\frac{a}{\pi\sigma}\sin\pi x^* C_1(z^*)\cos t^* \tag{16}$$

$$\phi_2=-\frac{a^2}{16\sigma}\{B_{02}+B_{22}\cos 2\pi x^* C_2(z^*)\}\sin 2t^* \tag{17}$$

$$\begin{aligned}\phi_3=\frac{\pi a^3}{256\sigma}\{&-B_{31}\sin 3\pi x^* C_3(z^*)\cos t^*\\&+B_{13}\sin\pi x^* C_1(z^*)\cos 3t^*+B_{33}\sin 3\pi x^* C_3(z^*)\cos 3t^*\}\\&+\frac{4}{\pi^2}\sum_{n=2}^{\infty}\frac{(-1)^{n-1}\sin(2n-1)\pi x^*}{(2n-1)^2\{(\omega_{2n-1}/\omega_1)^2-1\}}C_{2n-1}(z^*)\cos t^*\end{aligned} \tag{18}$$

$$\eta_1=a\sin\pi x^*\sin t^* \tag{19}$$

$$\eta_2=a^2 A_{22}\cos 2\pi x^*\cos 2t^* \tag{20}$$

$$\begin{aligned}\eta_3=&a^3 A_{11}\sin\pi x^*\sin t^*-a^3 A_{31}\sin 3\pi x^*\sin t^*\\&+a^3 A_{13}\sin\pi x^*\sin 3t^*+a^3 A_{33}\sin 3\pi x^*\sin 3t^*\\&+\frac{2\sigma}{\pi}\sin\pi x^*\sin t^*\\&+\frac{4\sigma}{\pi}\sum_{n=2}^{\infty}\frac{(-1)^{n-1}\sin(2n-1)\pi x^*}{(2n-1)^2\{1-(\omega_1/\omega_{2n-1})^2}\sin t^*\end{aligned} \tag{21}$$

where a corresponds to the free surface elevation and satisfies the following equation:

$$R\varepsilon^3 a^3-\left(\frac{\omega}{\omega_1}-1\right)\varepsilon a-\frac{2\sigma X_0}{\pi L}=0 \tag{22}$$

Finally, σ, $C_n(z^*)$, R, A_{ij} and B_{ij} are

$$\sigma=\tanh(\pi h/L)$$

$$C_n(z^*)=\frac{\cosh n\pi(z^*+h/L)}{\cosh n\pi h/L}$$

$$R=\frac{\pi^2}{64}(9\sigma^{-4}-14\sigma^{-2}-3)$$

$$A_{11}=\frac{\pi^2}{64}(3\sigma^{-4}+12\sigma^{-2}-1)$$

$$A_{13}=\frac{\pi^2}{256}(9\sigma^{-4}+54\sigma^{-2}-15)$$

$$A_{22}=\frac{\pi}{8}(3\sigma^{-3}-\sigma^{-1})$$

$$A_{31}=\frac{\pi^2}{256}(27\sigma^{-4}+51\sigma^{-2}-87-15\sigma^2)$$

$$A_{33}=\frac{\pi^2}{256}(81\sigma^{-6}-27\sigma^{-4}+27\sigma^{-2}-9)$$

$$B_{02}=3\sigma+\sigma^{-1}$$

$$B_{13}=9\sigma^{-4}+62\sigma^{-2}-31$$

$$B_{22}=3(\sigma^{-3}-\sigma)$$

$$B_{31}=3\sigma^{-4}+11\sigma^{-2}+1-15\sigma^2$$

$$B_{33}=9\sigma^{-6}+5\sigma^{-4}-53\sigma^{-2}+39$$

4 Results and discussions

The frequency response of the free surface of a magnetic fluid is shown in Fig. 5. Here B is the surface magnetic field induction at the center of the permanent magnet, η is the maximum free surface elevation at the side wall and ω_E is the first resonant angular frequency obtained by experiment for $B=0$. As the forcing frequency increases, the surface elevation also increases until the free surface is intensively shaken near the resonant frequency. After the resonant frequency, the surface disturbance is repressed. The first resonant frequency shifts to a higher frequency as the magnetic field intensity is increased. Assuming a potential flow and using a perturbation method, we have obtained nonlinear sloshing responses up to the third order perturbation $O(\varepsilon^3)$ as mentioned above. In Fig. 6 experimental results are compared with the linear and nonlinear theoretical results for $B=0$, 40, and 80 mT. Here ω_0 is the first resonant angular frequency obtained by the linearized wave theory when there is no magnetic field. In the low frequency range, the nonlinear solution is larger than the experimental values because calculated amplitude does not become zero with a decrease of the frequency (Hayama et al.

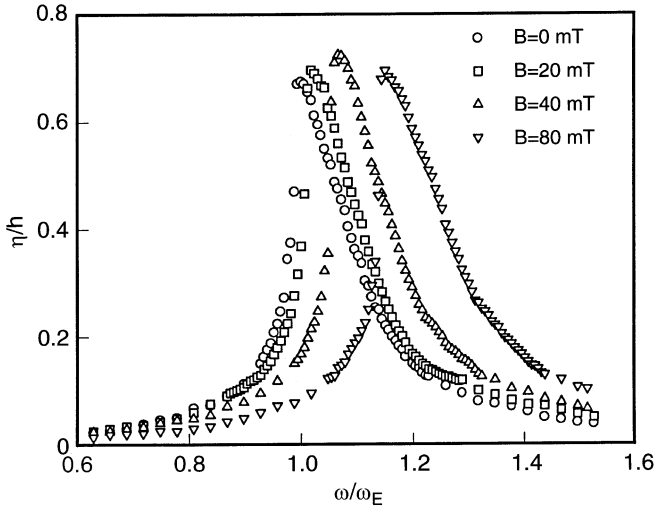

Fig. 5. Frequency response of the free surface

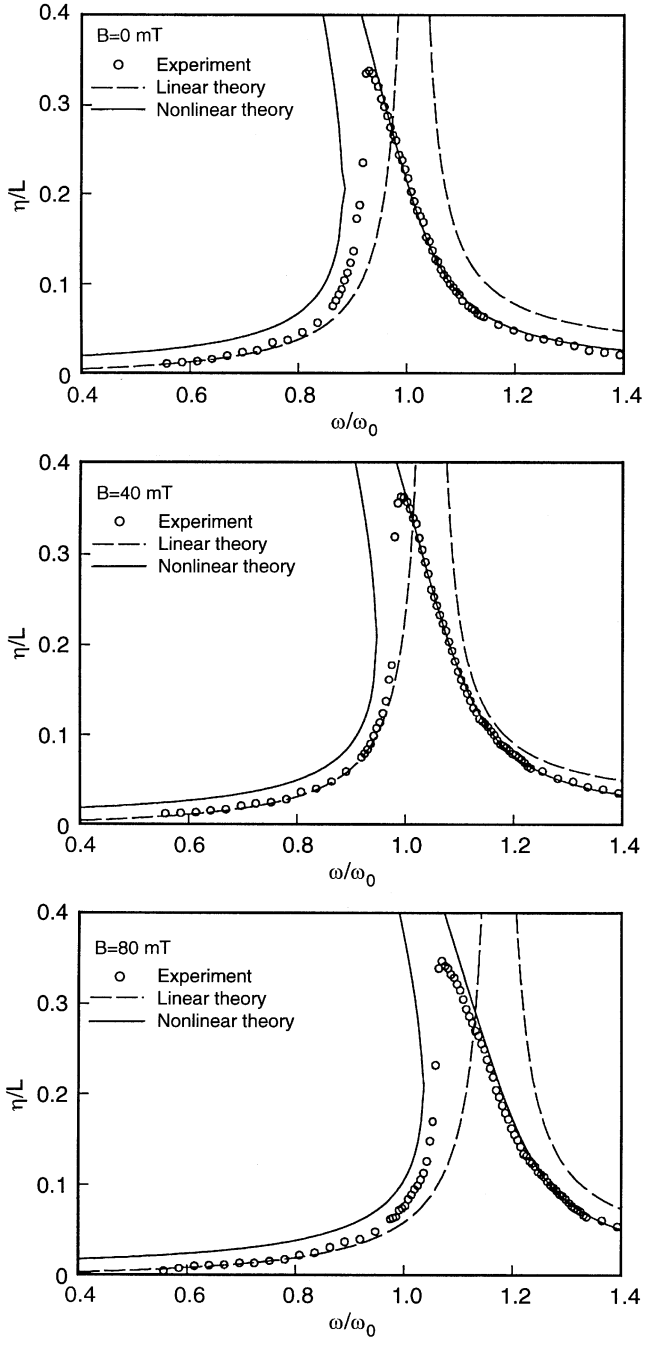

Fig. 6. Comparison of theoretical and experimental results for frequency response of surface elevation

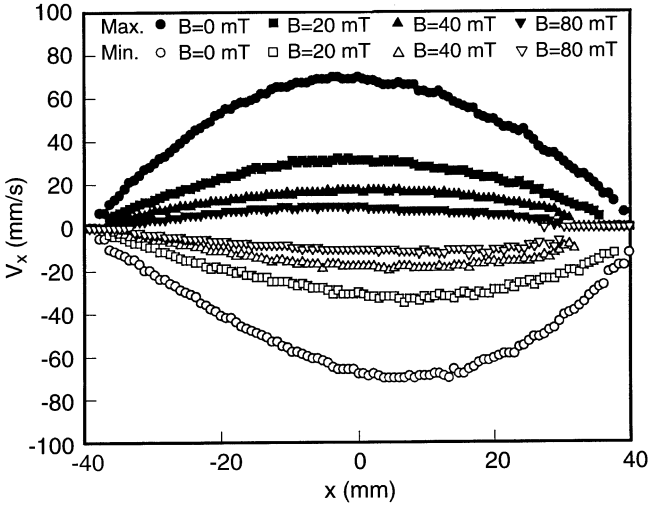

Fig. 7. Velocity profiles for $f=2.75$ Hz at $h_z=10$ mm

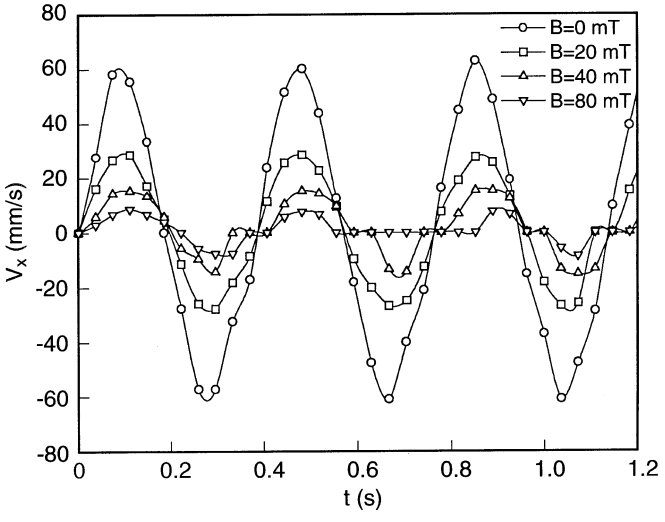

Fig. 8. Time dependent velocity profiles for $f=2.75$ Hz at $x=-0.04$ mm and $h_z=10$ mm

1983). Experimental and nonlinear theoretical results have a good agreement particularly, in the high frequency region.

UVP measurements were mainly carried out at near-resonant frequencies. Figure 7 shows the maximum and minimum velocity profiles for several applied magnetic fields. There are 1024 measurement points along the measurement axis, each representing the velocity value over a 39 ms period. Here h_z is the position of the ultrasonic transducer from the bottom wall. The time-dependent velocity profiles at a point, $x=-0.04$ mm, are illustrated in Fig. 8. The resonant frequency obtained by experiment for $B=0$ is $f=2.75$ Hz. Positive velocity means a flow direction away from the ultrasonic transducer. When the magnetic field increases, the velocity decreases because of the magnetic force. That is, the effective gravity increases as expressed in Eq. (9). The increase in effective gravity also causes the ultrasound reflecting particles to float upward, consequently echo signals are not received by the ultrasonic transducer. The absence of velocity data, especially for $B=80$ mT, in Figs. 7 and 8 results from this rise of reflecting particles. The spatial velocity profiles which is not symmetric with respect to the central axis ($x=0$) (as shown in Fig. 7) is caused by the nonlinearity of fluid motion.

From the measured velocity data, we calculated 128 power spectra by using a fast Fourier transform in the time domain. Figure 9 shows the power averaged over a central region (-9.6 mm $\leqslant x \leqslant 10.32$ mm, $h_z=10$ mm). The most dominant peak is f_1, which corresponds to the forcing frequency. The peaks f_2 and f_3 represent two and three times the forcing frequency, respectively. The height of each peak decreases with

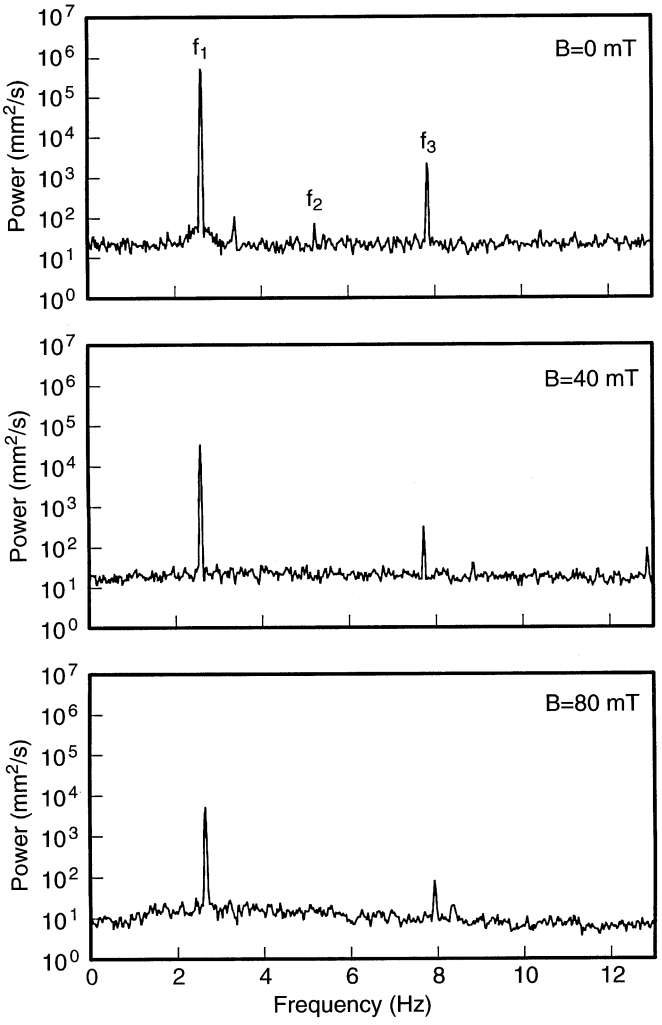

Fig. 9. Averaged power spectra for $f=2.75$ Hz over the range $-9.6\ \text{mm} \leqslant x \leqslant 10.32\ \text{mm}$ at $h_z=10$ mm

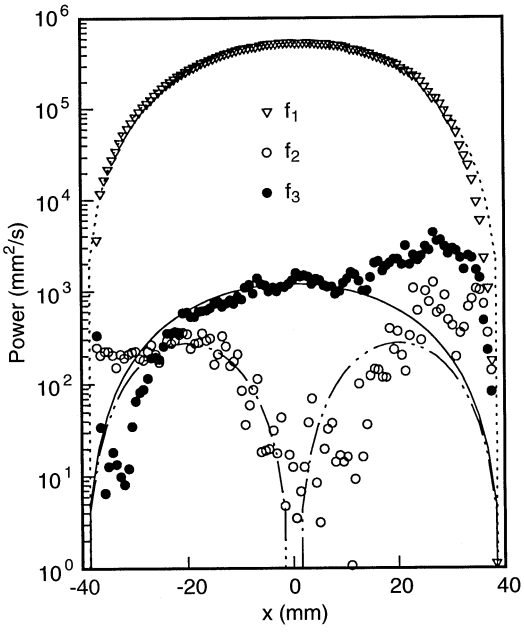

Fig. 10. Spatial distribution of the power spectra for $f=2.93$ Hz and $B=40$ mT

increasing magnetic field intensity because the disturbance of the fluid is suppressed by the magnetic field.

Figure 10 illustrates time averaged spatial distributions of the power spectra for f_1, f_2 and f_3 at a resonant state ($f=2.93$ Hz) for $B=40$ mT. Using the velocity potential derived from theory, the dimensionless velocity component in the x direction is given by

$$v_x^\star = \frac{v_x}{L\omega_1} = \frac{\partial \phi^\star}{\partial x^\star} \tag{23}$$

In Fig. 10, the nonlinear theoretical spatial spectra for f_1, f_2 and f_3 obtained by Eq. (23) are shown by a broken line, a chain line with two dots, and a solid line, respectively. The distribution of the frequency component f_1 are in agreement with the theoretical results. However, the other power spectra deviate from the theoretical lines, especially near the side wall furthest from the ultrasonic transducer. This may be because the ultrasonic echo signal diminishes at these distances; that is, due to the clustering and chaining of the magnetic particles that occurs under an applied magnetic field (e.g. Rosensweig 1985). If the ultrasound reflecting particles are too small, reflection efficiency becomes lower and the energy of echo is too small to maintain a high S/N ratio. If the particles are larger, the probability of multiple reflection between particles becomes higher which would result in a distortion of the velocity profile. We can not understand the effective size of the ultrasound reflecting particles under the magnetic fluid. That remains to be solved in future.

5
Concluding remarks

Lateral sloshing of a magnetic fluid in a rectangular container in a vertically-applied non-uniform magnetic fields has been investigated. Assuming a potential flow and using a perturbation method, we have obtained nonlinear sloshing responses up to the third order perturbation in the vicinity of the first resonant frequency. The theoretical nonlinear solutions agree with the experimental results. However, the nonlinear solutions are a little larger than the experimental data in the lower frequency range because the amplitude of the free surface oscillation does not become zero with a decrease of the frequency. In fact, in this range, the linear solutions are in better agreement with the experimental values.

Since the magnetic fluid is opaque, it has been very difficult to obtain velocity field data using a conventional measuring technique. We have applied the ultrasound velocimetry to a sloshing liquid to obtain both spatial velocity profiles along horizontal lines and time dependent velocity profiles. The amplitude of the velocity decreases with a increase in magnetic field intensity because of increase of the magnetic force. Also, the power spectra were calculated from the velocity data. The spatial distribution of the dominant peak f_1 are in good agreement with the nonlinear theoretical results, however, other power spectra deviate from the theoretical lines. In the future, we suggest the investigation of the influence of

magnetic fields on ultrasound reflecting particles and the clustering mechanism of magnetic ultrasound reflecting particles.

References

Dean RG; Dalrymple RA (1984) Water wave mechanics for engineers and scientists. Chap. 3, Prentice-Hall, Englewood Cliffs NJ

Dodge FT; Garza LR (1970) Magnetic fluid simulation of liquid sloshing in low gravity. NASA Tech Rep 9: 1–29

Handa K; Tajima K (1979) Sloshing of two superposed liquid layers in a rectangular tank. Trans Jpn Soc Mech Eng 45 B: 1450–1457

Hashimoto H; Sudo S (1985) Dynamic behavior of stratified fluids in a rectangular container subject to vertical vibration. Bull JSME 28: 1910–1917

Hayama S; Aruga K; Watanabe T (1983) Nonlinear researches of sloshing in rectangular tanks (1st Report, Nonlinear responses of surface elevation). Bull JSME 26: 1641–1648

Kikura H; Sawada T; Tanahashi T (1991) Surface behavior of magnetic fluid sloshing and its frequency responses. Trans Jpn Soc Mech Eng 57 B: 1629–1634

Li CH (1970) Instability of time-periodic flows of stratified fluids. Phys Fluid 13: 1121–1134

Matsuura F; Matsubara Y; Sawada T; Tanahashi T (1995) Surface behaviors of two-layers liquid sloshing under non-uniform magnetic field. In: Advanced computational and design techniques in applied electronic systems. (ed Hahn SY), pp 517–520, Elsevier Science, Amsterdam

Okubo M; Ishibashi Y; Oshima S; Katakura H; Yamane R (1990) Interfacial waves of the magnetic fluid in vertical alternating magnetic fields. J Magn Magn Mat 85: 163–166

Rosensweig RE (1985) Ferrohydrodynamics. Cambridge: Cambridge University Press

Sawada T; Kikura H; Shibata S; Tanahashi T (1993) Lateral sloshing of a magnetic fluid in a container. J Magn Magn Mat 122: 424–427

Sudo S; Hashimoto H; Katagiri K (1987) Interfacial instability of magnetic fluids in a rectangular container. JSME Int J 30: 1086–1092

Takeda Y (1986) Velocity profile measurement by ultrasound Doppler shift method. Int J Heat Fluid Flow 7: 313–318

Takeda Y (1987) Measurement of velocity profile of mercury flow by ultrasound Doppler shift method. Nuc Technol 79: 120–124

Zelazo RE; Melcher JR (1969) Dynamics and stability of ferrofluids surface interaction. J Fluid Mech 39: 1–24